



Article

Aerosol Characteristics and Their Impact on the Himalayan Energy Budget

Kesar Chand ¹, Jagdish Chandra Kuniyal ^{2,*}, Shruti Kanga ³, Raj Paul Guleria ⁴, Gowhar Meraj ⁵, Pankaj Kumar ^{6,*}, Majid Farooq ⁵, Suraj Kumar Singh ⁷, Mahendra Singh Nathawat ⁸, Netrananda Sahu ⁹ and Raj Kumar ¹⁰

¹ North East Regional Center, G.B. Pant National Institute of Himalayan Environment (NIHE), Itanagar 791113, Arunachal Pradesh, India; kesar.chand@gbpihed.nic.in

² G.B. Pant National Institute of Himalayan Environment (NIHE), Kosi-Katarmal, Almora 263643, Uttarakhand, India

³ Centre for Climate Change and Water Research, Suresh GyanVihar University, Jaipur 302017, Rajasthan, India; shruti.kanga@mygyanvihar.com

⁴ Directorate of Higher Education Shimla, Government of Himachal Pradesh, Lalpani, Shimla 171001, Himachal Pradesh, India; rpguleria_raj@yahoo.com

⁵ Department of Ecology, Environment and Remote Sensing, Government of Jammu and Kashmir, Srinagar 190018, Jammu and Kashmir, India; gowharmeraj@gmail.com (G.M.); majid_rsgis@yahoo.com (M.F.)

⁶ Institute for Global Environmental Strategies, Hayama 240-0115, Kanagawa, Japan

⁷ Centre for Sustainable Development, Suresh Gyan Vihar University, Jaipur 302017, Rajasthan, India; suraj.kumar@mygyanvihar.com

⁸ Department of Geography, Indira Gandhi National Open University (IGNOU), Maidan Garhi Rd, Maidan Garhi, New Delhi 110068, India; msnathawat@ignou.ac.in

⁹ Department of Geography, Delhi School of Economics, University of Delhi, Delhi 110007, India; nsahu@geography.du.ac.in

¹⁰ Department of Physics, Government Degree College Jukhala, Bilaspur 174001, Himachal Pradesh, India; rkb.66@redifmail.com

* Correspondence: jckuniyal@gbpihed.nic.in (J.C.K.); kumar@iges.or.jp (P.K.)



Citation: Chand, K.; Kuniyal, J.C.; Kanga, S.; Guleria, R.P.; Meraj, G.; Kumar, P.; Farooq, M.; Singh, S.K.; Nathawat, M.S.; Sahu, N.; et al. Aerosol Characteristics and Their Impact on the Himalayan Energy Budget. *Sustainability* **2022**, *14*, 179. <https://doi.org/10.3390/su14010179>

Academic Editor: Grigoris L. Kyriakopoulos

Received: 18 September 2021

Accepted: 23 December 2021

Published: 24 December 2021

Publisher's Note: MDPI stays neutral with regard to jurisdictional claims in published maps and institutional affiliations.



Copyright: © 2021 by the authors. Licensee MDPI, Basel, Switzerland. This article is an open access article distributed under the terms and conditions of the Creative Commons Attribution (CC BY) license (<https://creativecommons.org/licenses/by/4.0/>).

Abstract: The extensive work on the increasing burden of aerosols and resultant climate implications shows a matter of great concern. In this study, we investigate the aerosol optical depth (AOD) variations in the Indian Himalayan Region (IHR) between its plains and alpine regions and the corresponding consequences on the energy balance on the Himalayan glaciers. For this purpose, AOD data from Moderate Resolution Imaging Spectroradiometer (MODIS, MOD-L3), Aerosol Robotic Network (AERONET), India, and Cloud-Aerosol Lidar and Infrared Pathfinder Satellite Observation (CALIPSO) were analyzed. Aerosol radiative forcing (ARF) was assessed using the atmospheric radiation transfer model (RTM) integrated into AERONET inversion code based on the Discrete Ordinate Radiative Transfer (DISORT) module. Further, air mass trajectory over the entire IHR was analyzed using a hybrid Single-Particle Lagrangian Integrated Trajectory (HYSPPLIT) model. We estimated that between 2001 and 2015, the monthly average ARF at the surface (ARFSFC), top of the atmosphere (ARFTOA), and atmosphere (ARFATM) were $-89.6 \pm 18.6 \text{ W m}^{-2}$, $-25.2 \pm 6.8 \text{ W m}^{-2}$, and $+64.4 \pm 16.5 \text{ W m}^{-2}$, respectively. We observed that during dust aerosol transport days, the ARFSFC and TOA changed by -112.2 and -40.7 W m^{-2} , respectively, compared with low aerosol loading days, thereby accounting for the decrease in the solar radiation by 207% reaching the surface. This substantial decrease in the solar radiation reaching the Earth's surface increases the heating rate in the atmosphere by 3.1-fold, thereby acting as an additional forcing factor for accelerated melting of the snow and glacier resources of the IHR.

Keywords: aerosol; climate; AERONET; MODIS; CALIPSO; radiative forcing; Himalayas

1. Introduction

Climate change has been mainly attributed to increased atmospheric greenhouse gases (GHGs) leading towards a warming climate. Apart from GHGs, scientists are also assessing the impact of aerosols in acting as the agents of the warming climate as a result of their established function in affecting the atmospheric energy balance and thus directly affecting global climate model (GCM) predictions. This uncertainty in the GCM projections is partly incorporated by an incomplete understanding of how aerosols affect various climate system components. Aerosols are tiny particles existing in solid, liquid, or gaseous phases (from 0.001 μm to 100 μm), getting circulated between the land surface and stratosphere [1,2]. Biomass burning, mineral dust, volcanic eruptions, and incomplete combustion of fossil fuels are prominent sources of atmospheric aerosols [2,3]. Aerosols of anthropogenic origin influence the microclimatic system through their absorption and scattering of incoming solar radiations [4–6].

Aerosols interact with incoming solar radiations, either by the way of scattering or absorption, leading to either a cooling or warming effect on the atmosphere's overall energy budget, respectively [7,8]. It further depends on the land surface and cloud properties. As a result of this interaction, various global atmospheric processes such as regional and local hydrological cycles [9], monsoons [10], and vertical atmospheric heating profiles are affected [11]. On land, due to the warming effect of aerosols, a direct impact in the form of the accelerated melting of glaciers has been reported [11]. Hence, studying atmospheric aerosol and its impact on certain regions of the Earth, considering the indicator-regions of climate change, such as the Himalayas, has been at the forefront of recent studies in climate change science. Studies have concluded with substantial evidence regarding the role of aerosols in inducing tropospheric heating results in the alpine regions of the Himalayas along with their elevated sites [12].

In this work, we made an attempt to understand co-variability between aerosols originating over West Africa and West Asia and appearing heavy loads of aerosols over the Arabian Peninsula and hence its role in generating a dusty aerosol layer along the northwestern part of Indian Himalaya foothills. This dusty layer forms a layer of aerosols along the foothills of the Indian Himalaya and gives rise to the mechanism so-called "elevated heat pump" [13]. This mechanism amplifies the seasonal heating along with the elevated sites of the Indian Himalaya, leading to increased tropospheric warming, particularly from April to June [14–17], subsequently amplifying and strengthening the monsoon rainfall over northern India between June and July.

Anthropogenic distinctive aerosols have dominated and influential contribution in the microclimatic system through their absorption and scattering properties to solar radiation. This study provides important insight for carrying out studies on the transport of aerosols and their impact over the Himalayan region [7,8]. The scientific research of aerosol characteristics and transportation to the sensitive geographical part of the globe makes us clear about atmospheric warming, glacier retreat, and regional climate change [18]. A holistic assessment of the aerosol optical and transportation can improve the modeling of aerosol effects and variations in the albedo of snow/glaciers over the Trans-Himalayan region [19]. The emission of anthropogenic particles accelerates the changes in the critical physical signature of the Himalayan Mountain ranges, which is nowadays called the aerosol factory of the globe [20]. It has been seen the impacted region over the world due to implications due to climate change in the Himalayan ranges [21–23]. This study presents the long-term aerosol radiative variability and optical characteristics like aerosol radiative forcing (ARF). These hilly and fragile mountain ranges show the influence of anthropogenic aerosol and their role in ascendancy solar radiation.

2. Materials and Methods

The information on aerosol optical characteristics was gathered from three datasets, AERONET L2, MODIS L3, and CALIPSO, in order to meet the study's goals. The AErosol Robotic NETwork (AERONET) initiative is a worldwide chain of ground-based solar

photometers used to detect optical aerosol characteristics such as aerosol optical depth (AOD) and aerosol size dispensing (ASD). AERONET collects worldwide estimations of aerosol optical properties in a variety of aerosol systems with high temporal resolution [24]. The AERONET network uses CIMEL sun/sky spectral radiometers to analyze incoming solar radiation extinction at eight wavelengths 0.34, 0.38, 0.44, 0.5, 0.67, 0.87, 0.94, and 1.020 m.

Since 1999, MODIS, onboard NASA's Terra polar-orbiting satellite, has been operational. The Terra satellite allows researchers to examine aerosol from orbit with remarkable precision, almost on a worldwide scale [19]. On a daily basis, MODIS onboard Terra scans the Earth with a swath of 2330 km, allowing it to measure AOD with near-global coverage. Terra runs at 705 km altitude, climbing to the north at 10:30 IST equatorial crossing time. MODIS is a well-calibrated spectroradiometer with 36 spectral channels ranging from 0.41 to 14.4 m. The MODIS method is based on spectral reflectance, which depends on spectral radiance, L_λ , the Sun's zenith angle (θ), and irradiance f_0 at wavelength, and is connected by the equation:

$$\rho_\lambda = L_\lambda \frac{\pi}{f_{0,\lambda} \cos(\theta)} \quad (1)$$

The λ in the equation has been adjusted in the MODIS AOD products to specifically capture the interaction with the atmospheric aerosols.

The spatial resolutions are 1000 m, 500 m, and 250 m with 29, 5, and 2 spectral bands, respectively [25]. Here, MODIS daily level-3, 005 AOD data (550 nm) at a 1° latitude/longitude grid were averaged to generate daily MOD08_D3.005 and MYD08_D3.051 data products from Terra and Aqua satellites, respectively. Terra and Aqua operate at an altitude of 705 km, with equatorial passing time at 10:30 Indian Standard Time (IST) ascending towards the north and at 13:30 IST plunging towards the south [26], confirming that the AOD values regained from MODIS are correct within an uncertainty perimeter of

$$\Delta \tau p \lambda = \pm 0.05 \pm 0.15 \text{ } \tau p \lambda \text{ over land,} \quad (2)$$

where $\tau p \lambda$ is the ground-based AOD value. The data from Terra and Aqua measured at two different times on a day were combined to obtain the daily mean AOD for that day [27].

The CALIPSO satellite (launched April 2006) used to examine the role of clouds and aerosols in Earth's climate regulation. CALIPSO has a 98° orbit inclination, orbiting at 705 km and disseminating daily worldwide distribution of clouds and aerosols [21]. CALIPSO carries Cloud-Aerosol Lidar with Orthogonal Polarization (CALIOP), is an imaging Infrared Radiometer (IIR), and a moderate spatial resolution Wide Field-of-view Camera (WFC) has depolarization corresponding to wavelength 532 nm that are proficient of discriminating amongst ice and water clouds and identifying non-spherical aerosol particles. As a result of this benefit, CALIOP is favored to quantify the vertical structure of dust plumes directly. Here, we used CALIPSO to supplement observations of aerosol acquired by the MODIS.

The ARF calculation algorithm was developed by Kimet et al. as follows [28]:

$$F = -\frac{S}{4} T^+ T^- (1 - N) 2\tau \left[(1 - \alpha)^2 \beta \omega - 2\alpha(1 - \omega) \right] \quad (3)$$

where F is the radiative forcing (W/m^2), S incident solar flux at TOA, T^+ and T^- are the upward and downward transmissions, N cloudiness index, τ AOD, α albedo (surface), β radiation scattered as fraction upwards, and ω is the single albedo aerosol scattering.

Using AERONET retrieved aerosol optical depth, fundamental part and imaginary part natural refractive index (or single scattering albedo) at 500 nm, and volume size distribution, radiative transfer model calculates solar direct and diffuse flux. The estimated solar fluxes are related to variations in solar fluxes. This process changes the water vapor ratio of the refractive index. The transfer radiative model calculates aerosol radiative forcing at the

top of the atmosphere and the surface using an adjusted sky radiometer measured aerosol optical properties. The Santa Barbara DISORT Atmospheric Radiative Transfer (SBDART) model is used to recreate the solar irradiance over the study area at the surface, within the atmosphere, and over top of the atmosphere (TOA). The SBDART is used to solve radiative transfer algorithms to estimate the radiative effects of atmospheric boundary layers [29]. The essential info parameters utilized in the SBDART for forcing estimations are SSA, asymmetry parameter (AP), and AOD. Aerosol Radiative Forcing (ARF) depicts the influence of aerosols on the absorption and scattering of solar radiations. The positive values of ARF indicate the warming, and negative values indicate the cooling.

In this study, these parameters were obtained from the OPAC database [30]. Here, we make use of OPAC (Optical Properties of Aerosol and Clouds version) using Ångström exponent associated with the matching absorption coefficient. Further, using the Discrete Ordinate Radiative Transfer module, the clear-sky SWARF calculations in the shortwave region, i.e., 0.25–4.0 μm , are made by using the radiative transfer model (RTM) [29]. Spectral AOD and SSA used as input in RTM were estimated from the OPAC database at wavelength of 0.25–4.0 μm .

3. Results

3.1. A View of Global Aerosol Characteristics

Figure 1 is drawn to illustrate seasonal changes in aerosol characteristics, i.e., aerosol optical depth (AOD) at 0.55 μm wavelength. From the figure, it depicts that the distribution of aerosols is not uniform. The continental aerosol plumes disperse over a wider area of oceanic regions. MODIS observations recognize that the Sahara dust plume is the globally distributed aerosol plume and is extended to several thousand kilometers over the Atlantic Ocean. MODIS observations also identified a few more aerosol hotspots, such as the Taklamakan region, the eastern part of China, the tropical part of Africa, the Arabian Sea, and Indo-Gangetic Plains (IGP). The AOD over these aerosol hotspots regions in most of the months of the year remains more significant than 0.6.

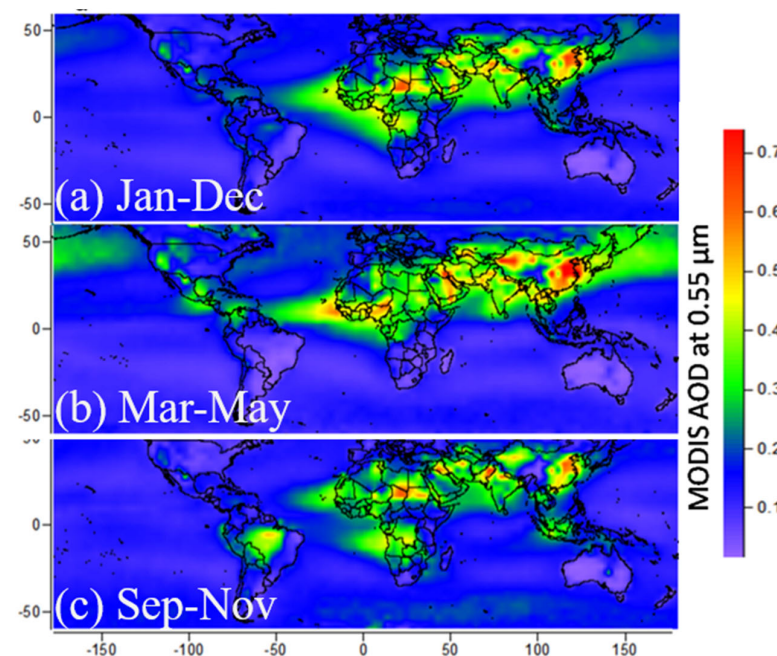


Figure 1. Characteristics of global AOD at 0.55 μm wavelength (period: 2000–2013).

Moreover, atmospheric changes due to aerosols are operative in these aerosol hotspots areas [31]. The AOD characteristics for the period of March–May were found different from that of September–November. The seasonal biomass burning, particularly during

September–November, is eye-catching over the Amazon basin in South America and South Africa [32,33]. This feature reflects the seasonal dependent behavior of AOD characteristics. The seasonal dependent behavior of AOD characteristics can also be seen over the Mediterranean and the Arabian Sea, as reported by Sheel et al. [25].

3.2. A View of Regional Aerosol Characteristics: Indian Region

The maps of regional AOD characteristics over the Indian region depict that the aerosol distribution pattern is more or less similar in all years (Figure 2). These maps are drawn using an integrated approach of MODIS sensors, i.e., Dark Target and Deep Blue, which have separate land and ocean algorithms. There can be noticed with a decreasing pattern in aerosol distribution from 2003 to 2007, whereas there observed no significant change over the Arabian Sea with shifts to higher aerosol loadings. The signatures of aerosol burden over the Arabian Sea before and after 2007 are distinguishable. The satellite maps suggest heavy dust storms after 2007 [34].

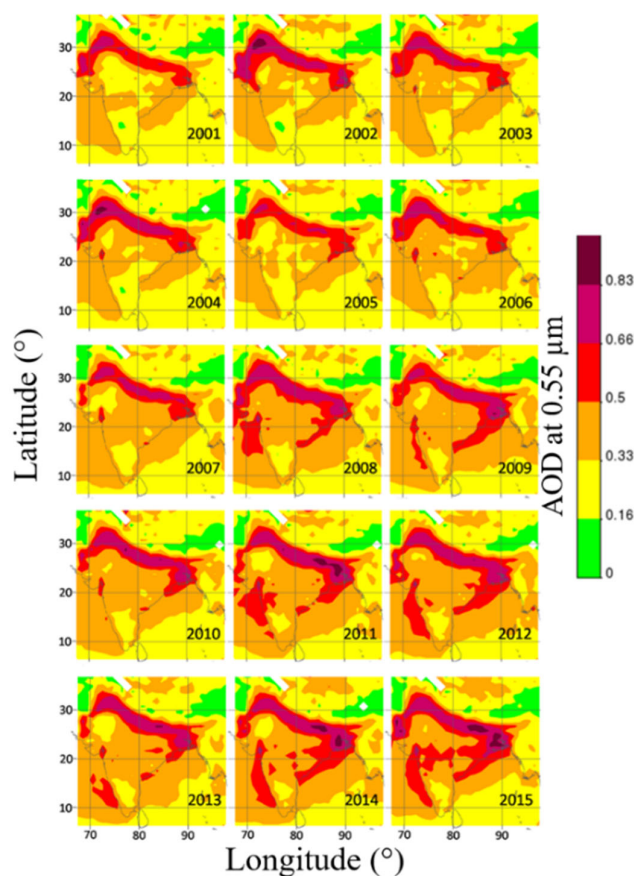


Figure 2. Time-averaged maps of Dark Target plus Deep Blue AOD at 0.55 μm wavelength for each year, i.e., from 2001 to 2015.

The western part of India, particularly Rajasthan, was observed with extensive aerosol loading followed by Gujarat. A slight decrease in annual mean AOD can be noticed in the following years, which could be related to enhanced forest cover and rainfall [35]. A moderate AOD can be seen over Madhya Pradesh and western Maharashtra. Eastern India comprises the IGP region and observes a heavy aerosol burden. The sizeable annual aerosol loading can be ascribed to its topography (i.e., northern plain and the elevated Himalayas), patterns of wind, and higher emissions from anthropogenic sources [36]. The amount of aerosol was noted over West Bengal, followed by Bihar and Jharkhand. The eastern states observe moderate to low aerosol loading. Satellite observations capture an increasing pattern from west to east, especially IGP. Southern India experiences a relatively

low aerosol burden. However, moderate to high aerosol loadings in surrounding oceanic regions can be observed. The Southern part of India (Kerala, Karnataka, and Tamil Nadu) experiences the lowest aerosol burden, particularly in the winter season, whereas the maximum is in the monsoon.

3.3. Observational Evidence of Aerosol Transport towards the Elevated Sites of the Himalaya

Figures 1 and 2 confirm that IGP is an aerosol hotspot area in the Himalayan foothills. The aerosol accumulated along the elevated sites of the Himalayas is mainly associated with desert dust [37], which is primarily transported from western regions [38]. These dust plumes are further transported towards elevated Indian Himalaya, imposing a severe threat to the Himalayan glaciers. The collective approach of HYSPLIT back-trajectory analysis, MODIS, and CALIPSO observations is a vital tool to identify aerosol sources employing transport from the distant source origin. This collective approach was previously used in numerous studies [39,40].

Globally, the incidences of events of dust storms are the most prevalent atmospheric phenomenon from March to June. The Sahara Desert, the Thar Desert of India, and the Arabian region are the primary origins of aerosols of desert dust. Desert dust originates over these regions and then is widely distributed by means of atmospheric transport. The observational evidence of atmospheric dust transport (dust plumes) is revealed from the satellite imaginaries (see Figure 3).

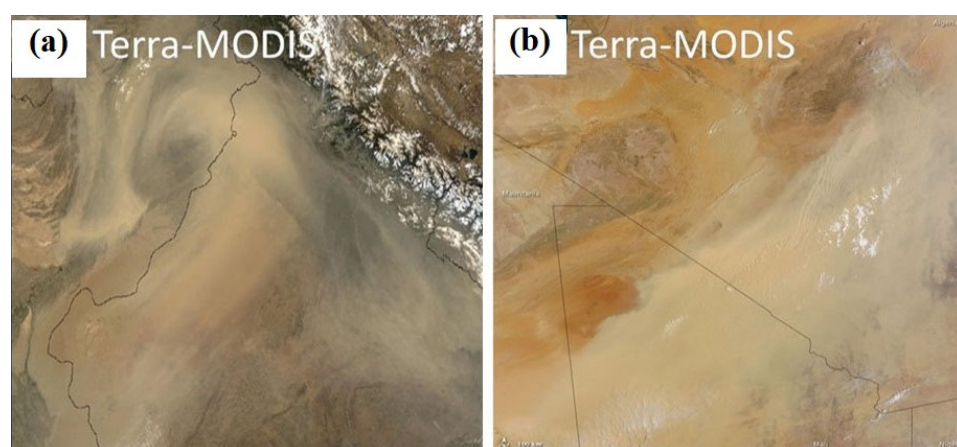


Figure 3. Satellite imaginaries showing transport of desert dust on (a) 9 June 2010 and (b) 10 June 2010 (Source: NASA Image Courtesy, 2010).

On 10 June 2010, the MODIS on the Terra satellite recorded a massive dust plume that swept across the Sahara Desert (Figure 3a). The plume spreads from Mauritania through Mali and into Algeria, appears only slightly brighter than the earth-toned terrain below. The dust plume develops unique wave patterns over Algeria, but it is thinner than it was over Mali. The dust storm's source locations aren't visible in this view, but vast sand seas engulf almost all of Mauritania, crossing the Mali–Algerian border. The original dust plumes are thought to have originated in the southwest and blown northeast, churning up further dust and dirt along the route. On 9 June 2010, thick clouds of desert dust blew across Pakistan (left) and India (right) in the base of the Himalayan Mountains (Figure 3b). The MODIS-Terra satellite obtained this image of the incident. On the snow-capped peaks of the Himalayas at the top right and the Indo-Gangetic Plain, the storm looks to be putting down a blanket of dust. We infer from satellite image analysis that many dust aerosols start over the Sahara, India's Thar Desert, and the Arabian area and then travel to the northern section of the country, impacting regional climate.

To investigate the influence of atmospheric dust transport in modulating the physical properties of aerosols, we took the example of a typical month, i.e., May 2016, and the

day of low aerosol loading (7 May 2016) and extensive aerosol loading (27 May 2016) are analyzed. The aerosol volume size distribution ($dV/d\ln R$) depicts aerosols' bi-modal structure (Figure 4). AERONET station installed at IIT Kanpur is one of the represented sites in IGP. The aerosol volume distribution is estimated from the spectral Sun and sky radiance data using a well-explained technique by Dubovik and King (2002) [41]. We found that during dust aerosol loading day, the volume concentration of aerosols in the size range of $1.3\text{--}8.0\ \mu\text{m}$ has increased significantly, implying the domination of coarse-mode particles. Dubovik et al. (2002) observed this type of volume size distribution for desert aerosols. For size particles $r < 1.0\ \mu\text{m}$, there is no significant variation, even during dust loading day, which results in atmospheric transport carrying desert dust (a source of coarse-mode aerosols). Similar results by Dey et al. (2004) report that during dust episode days, the concentration at coarse-mode rises three times, with little change in volume of fine particles [42]. The aerosol volume size exhibits two prominent characteristics: fine particles $r < 1.0\ \mu\text{m}$ and coarse particles $r > 1.0\ \mu\text{m}$.

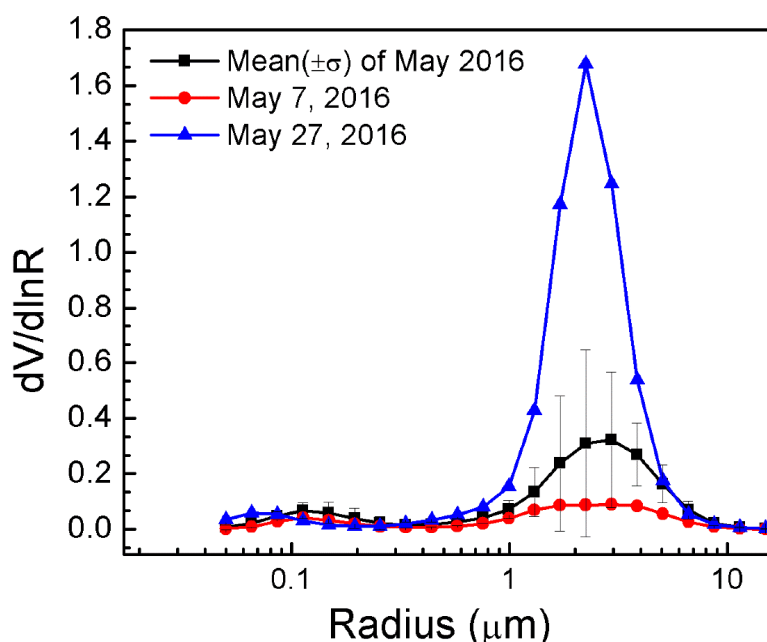


Figure 4. Characteristics of aerosol size distribution during low and significant aerosol loading days.

4. Discussion

Here, we investigate the influence of atmospheric dust transport on aerosol radiative forcing (ARF) over Kanpur. The significant aerosol loading day (27 May 2016) and low aerosol loading day (7 May 2016) are taken to observe the radiative effect of aerosols. The nearest CALIPSO pass transecting air parcels was available on 27 May 2016, at nighttime. The CALIPSO swath while passing from over India is shown in Figure 5. The air parcel (drawn at 5000 m above ground level) reached India on 27 May 2016 and was initiated from the Sahara. It after that passed via Saudi Arabia, Iran, and Afghanistan and created a vertical layer of dust aerosol over northern India.

Moreover, the air parcel travels the distance above the boundary layer. The boundary layer played an essential role in carrying the aerosol over a long distance. These features are explained by HYSPLIT back-trajectories connected with CALIPSO satellite observations in the events of dust aerosol loading day, i.e., 27 May 2016 (Figure 5). The air parcels suggest the western flow of air-born particles towards India.

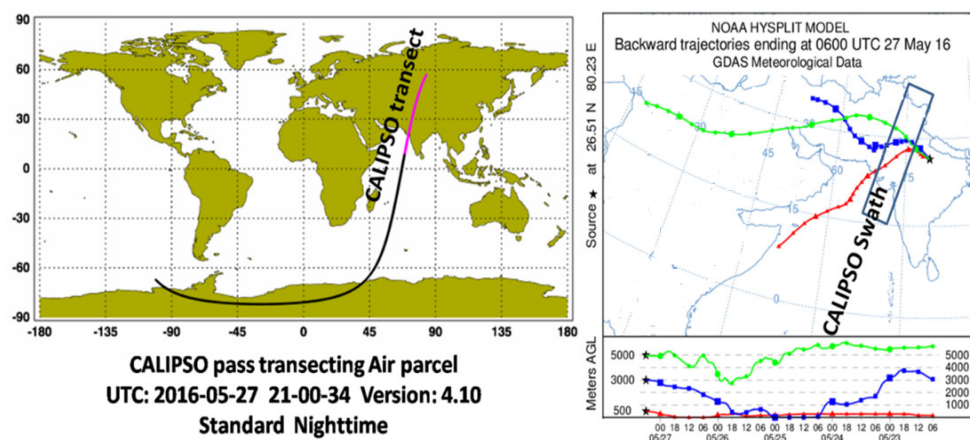


Figure 5. HYSPLIT back-trajectories investigating aerosol transport pathway coupled with CALIPSO satellite observations during dust aerosol loading day, i.e., 27 May 2016.

The air parcels reached Kanpur passed between Lat/Lon: 26/73 and 32/74 at the transect time of CALIPSO. The CALIPSO derived images investigated aerosol transport on 27 May 2016, while its transect in northern India is provided in Figure 5. The depolarization ratio is applied to distinguish different dust aerosols and is defined as the fraction of the perpendicular and the parallel components of the weakened backscatter signal. CALIPSO depolarization ratio image suggests a higher value > 0.4 near the surface (Figure 6a,b). Higher depolarization suggests a significant contribution of desert dust particles [38]. This feature is derived from CALIOP backscatter measurements, which realize that advected desert dust accompanies the near-surface aerosols. Figure 6c depicts a vertically extended tropospheric aerosol layer of ~ 7 km over northern India. The vertical profile of CALIPSO-derived image analysis has confirmed the dispersion of dust from the western deserts towards the north part of India (see Figure 6d).

In summary, on 27 May 2016, the western flow of air-born particles has amplified the likelihood of aerosol dust transport near Kanpur. On May 27, 2016, the AOD at 500 nm value was noted to be 313% higher when compared to low AOD day, i.e., 7 May 2016. About 90% decrease in α (440–870 nm) was estimated on 27 May 2016, as compared to 7 May 2016, which suggests a notable loading of dust. Figure 7 shows the status of ARF at TOA, SFC, and ATM. The influence of extensive aerosol loading can be revealed in Figure 7. It is found that atmospheric desert dust transport has a greater impact, with a notable decrease in surface-reaching solar radiation. During significant aerosol loading day, i.e., May 27, 2016, the desert dust transport causes a substantial decrease in the surface-reaching shortwave solar radiation by 166.4 W m^{-2} . During this day, the atmospheric aerosol radiative forcing increased by 106.3 W m^{-2} and translated into 2.98 K day^{-1} of atmospheric heating rate. The monthly average (mean $\pm \sigma$) value of ARF during May 2016 stood as $-24.4 \pm 14.8 \text{ W m}^{-2}$, $-109.5 \pm 35.4 \text{ W m}^{-2}$, and $83.1 \pm 38.4 \text{ W m}^{-2}$ at TOA, SFC, and ATM, respectively. Our work assessed that during DATD (dust aerosol transport day), the ARF at SFC and TOA vary by -112.2 and -40.7 W m^{-2} , respectively, against the low aerosol loading days.

This results in a considerable reduction in the surface-reaching solar radiation by 207%. Such a considerable reduction in the surface-reaching solar radiation enhances the atmospheric heating rate by 3.1-fold. A study to investigate the aerosol impact on surface incoming solar radiations was also performed by Prasad et al. (2007) from AERONET site Kanpur and showed that during dusty days, the average ARF at the SFC and TOA change by -23 and -11 W m^{-2} , respectively [43]. Nevertheless, the magnitude of reduction in present work is much higher than earlier work [43,44]. In summary, we conclude that aerosol has a profound impact in modulating aerosols' physical and radiative properties, which leads to climate forcing.

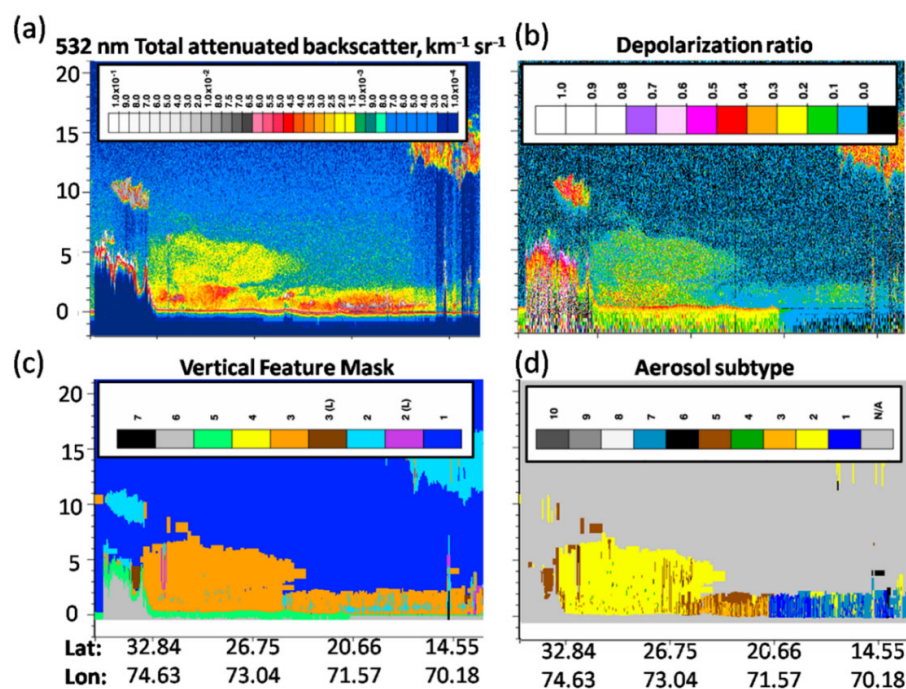


Figure 6. CALIPSO derived images investigating aerosol transport on 27 May 2016 while transect northern India. (a) Total attenuated backscatter, (b) depolarization ratio, (c) vertical feature mask (color bar: 1 clear air; 2 cloud; 3 tropospheric aerosol; 4 stratospheric aerosol; 5 surface; 6 subsurface; 7 totally attenuated), (d) aerosol subtype (color bar: 1 marine; 2 dust; 3 polluted continental/smoke; 4 clean continental; 5 polluted dust; 6 elevated smoke; 7 dusty marine; 8 PSC aerosol; 9 volcanic ash; 10 sulfate/other).

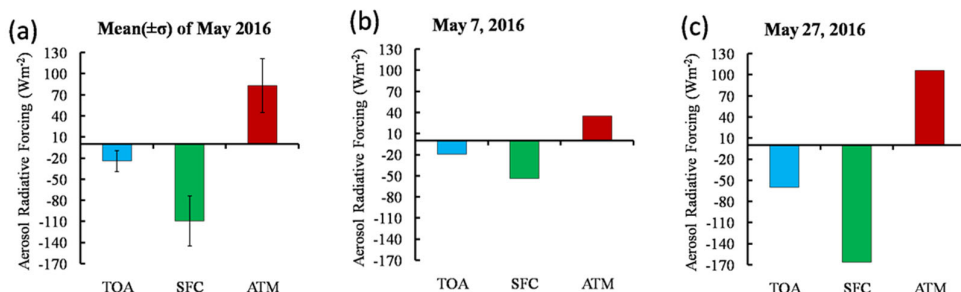


Figure 7. Aerosol radiative forcing during (a) May 2016 (mean $\pm \sigma$), (b) low aerosol loading day, and (c) significant aerosol loading day.

5. Conclusions

In 1993, National Aeronautics Space Administration (NASA) took the initiative to measure aerosols and launch a worldwide program called the AERONET program. Now with more than 500 AERONET stations, it is the world's most extensive program. The AERONET station at IIT Kanpur became operational on 22 January 2001. In India, it has been one of the ground stations monitoring aerosol for a long time. In recent years, numerous initiatives were also taken by the world's different agencies/organizations to monitor aerosol from space. Over India, satellite observations capture a decreasing pattern from 2003–2007, whereas there observed no significant change over the Arabian Sea. The variation in AOD was observed to be wavelength-dependent, showing seasonal dependence characteristics. The HYSPLIT trajectory analysis showed that the air masses that originate or pass through over western regions profoundly impact the Himalayan radiation budget. The ARF was analyzed to see the impact of aerosols on the Himalayan radiation budget. The monthly average ARF at the surface, within and, top-of-the atmosphere, was estimated

to be $-89.6 \pm 18.6 \text{ Wm}^{-2}$, $-25.2 \pm 6.8 \text{ Wm}^{-2}$, and $+64.4 \pm 16.5 \text{ Wm}^{-2}$, respectively. The above work examined that during dust aerosol transport day, the ARF at the surface and top-of-the atmosphere change by -112.2 and -40.7 Wm^{-2} , respectively, when results relate to declined aerosol loading day. In summary, we conclude that aerosol has a profound impact in modulating the radiation transfer, leading to climate forcing.

Author Contributions: Conceptualization, K.C., J.C.K., R.P.G. and R.K.; methodology, K.C., S.K., J.C.K., R.P.G. and G.M.; software, K.C., R.P.G., R.K. and G.M.; validation, K.C., J.C.K., R.P.G., R.K. and G.M.; formal analysis K.C., S.K., R.P.G., G.M., P.K., M.F., S.K.S., M.S.N., N.S. and R.K.; investigation, K.C., S.K., J.C.K., R.P.G., G.M., P.K., M.F., S.K.S., M.S.N. and N.S.; resources, K.C., J.C.K., P.K. and N.S.; data curation, K.C., S.K. and J.C.K.; writing—original draft preparation, K.C., S.K., J.C.K., R.P.G. and G.M.; writing—review and editing, K.C., S.K., J.C.K., R.P.G., G.M., P.K., M.F., S.K.S., M.S.N. and N.S.; visualization, K.C., J.C.K., R.P.G. and R.K.; supervision, K.C., J.C.K., R.P.G., M.F. and P.K.; project administration, J.C.K., P.K. and N.S.; funding acquisition, P.K. All authors have read and agreed to the published version of the manuscript.

Funding: Publication fund for this work is supported by Strategy Research Fund 2021 (WHN-Planetary-Health), an in-house grant from Institute for Global Environmental Strategies (IGES), Japan.

Institutional Review Board Statement: Not applicable.

Informed Consent Statement: Not applicable.

Data Availability Statement: The data can be shared on a special request to the corresponding authors.

Acknowledgments: We are thankful to the Director of G.B. Pant National Institute of Himalayan Environment (NIHE) for providing facilities in the Institute and the NASA Science team for providing satellite data obtained through MODIS and CALIPSO. The authors K.C. and J.C.K. are thankful to ISRO, Bengaluru for providing partial financial assistance to carry out the ‘aerosols climatology’ study under Aerosol Radiative Forcing over India (ARFI) under ISRO-GBP. We also acknowledge NOAA Air Resources Laboratory for providing the HYSPLIT transport model we have used in this work. We thank Brent Holben, a NASA Goddard Space Flight Center scientist, for deploying the CIMEL sun/sky spectral Sunphotometer under the AERONET program IIT Kanpur. Special thanks to S.N. Tripathi (Principal Investigator), Department of Civil Engineering, IIT Kanpur, and his staff for establishing and maintaining the Kanpur AERONET site used in this investigation. The author, G.M. is thankful to Department of Science and Technology, Government of India for providing the Young Scientist Fellowship under Scheme for Young Scientists and Technology (SYST-SEED) [Grant no. SP/YO/2019/1362(G) & (C)].

Conflicts of Interest: The authors declare no conflict of interest.

References

1. Pöschl, U. Atmospheric aerosols: Composition, transformation, climate and health effects. *Angew. Chem. Int. Ed.* **2005**, *44*, 7520–7540. [[CrossRef](#)] [[PubMed](#)]
2. Pósfai, M.; Buseck, P.R. Nature and climate effects of individual tropospheric aerosol particles. *Annu. Rev. Earth Planet. Sci.* **2010**, *38*, 17–43. [[CrossRef](#)]
3. Junge, C.E. *Air Chemistry and Radioactivity*; Academic Press: New York, NY, USA, 1963.
4. Ramanathan, V.; Carmichael, G. Global and regional climate changes due to black carbon. *Nat. Geos.* **2008**, *1*, 221. [[CrossRef](#)]
5. Stocker, T.; Qin, D.; Plattner, G.-K.; Tignor, M.; Allen, S.K.; Boschung, J.; Nauels, A.; Xia, Y.; Bex, V.; Midgley, P.M. (Eds.). *Intergovernmental Panel on Climate Change (IPCC), Climate Change 2013: The Physical Science Basis: Working Group I Contribution to the Fifth Assessment Report of the Intergovernmental Panel on Climate Change*; Cambridge University Press: New York, NY, USA, 2014; ISBN 978-1-107-05799-9.
6. Bond, T.C.; Doherty, S.J.; Fahey, D.W.; Forster, P.M.; Berntsen, T.; De Angelo, B.J.; Flanner, M.G.; Ghan, S.; Kärcher, B.; Koch, D.; et al. Bounding the role of black carbon in the climate system: A scientific assessment. *J. Geophys. Res.* **2013**, *118*, 5380–5552. [[CrossRef](#)]
7. Jiang, H.; Feingold, G. Effect of aerosol on warm convective clouds: Aerosol-cloud-surface flux feedbacks in a new coupled large-eddy model. *J. Geophys. Res.* **2006**, *111*, D01202. [[CrossRef](#)]
8. Fan, J.; Zhang, R.; Li, G.; Tao, W.-K.; Li, X. Simulations of cumulus clouds using a spectral microphysics cloud-resolving model. *J. Geophys. Res.* **2007**, *112*, D04201. [[CrossRef](#)]
9. Ramanathan, V.; Chung, C.; Kim, D.; Bettge, T.; Buja, L.; Kiehl, J.T.; Washington, W.M.; Fu, Q.; Sikka, D.R.; Wild, M. Atmospheric brown clouds: Impacts on South Asian climate and hydrological cycle. *Proc. Natl. Acad. Sci. USA* **2005**, *102*, 5326–5333. [[CrossRef](#)]

10. Vinoj, V.; Rasch, P.J.; Wang, H.; Yoon, J.H.; Ma, P.L.; Landu, K.; Singh, B. Short-term modulation of Indian summer monsoon rainfall by West Asian dust. *Nat. Geosci.* **2014**, *7*, 308–313. [[CrossRef](#)]
11. Lau, K.M.; Kim, M.K.; Kim, K.M.; Lee, W.S. Enhanced surface warming and accelerated snowmelt in the Himalayas and Tibetan Plateau induced by absorbing aerosols. *Environ. Res. Lett.* **2010**, *5*, 025204. [[CrossRef](#)]
12. Guleria, R.P.; Kuniyal, J.C.; Rawat, P.S.; Thakur, H.K.; Sharma, M.; Sharma, N.L.; Mahavir, S.; Chand, K.; Sharma, P.; Thakur, A.K.; et al. Aerosols optical properties in dynamic atmosphere in the northwestern part of the Indian Himalaya: A comparative study from ground and satellite-based observations. *Atmos. Res.* **2011**, *101*, 726–738. [[CrossRef](#)]
13. Lau, K.M.; Kim, K.M.; Kim, M.K. Asian monsoon anomalies induced by aerosol direct forcing: The role of the Tibetan Plateau. *Clim. Dyn.* **2006**, *26*, 855–864. [[CrossRef](#)]
14. Guleria, R.P.; Kuniyal, J.C.; Rawat, P.S.; Sharma, N.L.; Thakur, H.K.; Dhyani, P.P.; Singh, M. The assessment of aerosol optical properties over Mohal in the northwestern Indian Himalaya using satellite and ground based measurements and an influence of aerosol transport on aerosol radiative forcing. *Meteorol. Atmos. Phys.* **2011**, *113*, 1530169. [[CrossRef](#)]
15. Guleria, R.P.; Kuniyal, J.C.; Rawat, P.S.; Thakur, H.K.; Sharma, M.; Sharma, N.L.; Dhyani, P.P.; Singh, M. Validation of MODIS retrieval aerosol optical depth and an investigation on aerosol transport over Mohal in the northwestern Indian Himalaya. *Int. J. Remote Sens.* **2012**, *33*, 5379–5401. [[CrossRef](#)]
16. Guleria, R.P.; Kuniyal, J.C.; Dhyani, P.P. Validation of space-born Moderate Resolution Imaging Spectroradiometer remote sensors aerosol products using application of ground-based Multi-wavelength Radiometer. *Adv. Space Res.* **2012**, *50*, 1391–1404. [[CrossRef](#)]
17. Guleria, R.P.; Kuniyal, J.C. Characteristics of atmospheric aerosol particles and their role in aerosol radiative forcing over northwestern Indian Himalaya in particular and over India in general. *Air Qual. Atmos. Health* **2015**, *9*, 795–808. [[CrossRef](#)]
18. Sellegri, K.; Laj, P.; Venzac, H.; Boulon, J.; Picard, D.; Villani, P.; Vuillermoz, E.; Bonasoni, P.; Marinoni, A.; Cristofanelli, P. Seasonal variations of aerosol size distributions based on long-term measurements at the high altitude Himalayan site of Nepal Climate Observatory-Pyramid (5079 m), Nepal. *Atmos. Chem. Phys.* **2010**, *10*, 10679–10690. [[CrossRef](#)]
19. Pant, P.; Hegde, P.; Dumka, U.C.; Sagar, R.; Satheesh, S.K.; Moorthy, K.K.; Saha, A.; Srivastava, M.K. Aerosol characteristics at a high- altitude location in central Himalayas: Optical properties and radiative forcing. *J. Geophys. Res.* **2006**, *111*, D17206. [[CrossRef](#)]
20. Bianchi, F.; Kurtén, T.; Riva, M.; Mohr, C.; Rissanen, M.P.; Roldin, P.; Berndt, T.; Crounse, J.D.; Wennberg, P.O.; Mentel, T.F.; et al. Highly Oxygenated Organic Molecules (HOM) from Gas-Phase Autoxidation Involving Peroxy Radicals: A Key Contributor to Atmospheric Aerosol. *Chem. Rev.* **2019**, *119*, 3472–3509. [[CrossRef](#)] [[PubMed](#)]
21. Yamada, T.; Shiraiwa, T.; Iida, H.; Kadota, T.; Watanabe, T.; Rana, B.; Ageta, Y.; Fushimi, H. Fluctuations of the glaciers from the 1970s to 1989 in the Khumbu, Shorong and Langtang regions, Nepal Himalayas. *Bull. Glacier Res.* **1992**, *10*, 11–19.
22. Shrestha, A.B.; Wake, C.P.; Mayewski, P.A.; Dibb, J.E. Maximum temperature trends in the Himalaya and its vicinity: An analysis based on temperature records from Nepal for the period 1971–94. *J. Clim.* **1999**, *12*, 2775–2786. [[CrossRef](#)]
23. Hasnain, S.I. Himalayan glaciers meltdown: Impact on South Asian rivers. In *FRI 2002—Regional Hydrology: Bridging the Gap between Research and Practice*; van Lanen, H.A.J., Demuth, S., Eds.; IAHS Publication: Wallingford, UK, 2002; Volume 274, pp. 417–423. Available online: http://hydrologie.org/redbooks/a274/iahs_274_417.pdf (accessed on 17 September 2021).
24. Holben, B.N.; Eck, T.F.; Slutsker, I.; Tanre, D.; Buis, J.P.; Setzer, E.; Vermote, E.; Reagan, J.A.; Kaufman, J.A.; Nakajima, T.; et al. AERONET—a federated instrument network and data archive for aerosol characterization. *Remote Sens. Environ.* **1998**, *66*, 1–16. [[CrossRef](#)]
25. Sheel, V.; Guleria, R.P.; Ramachandran, S. Global and regional evaluation of a global model simulated AODs with AERONET and MODIS observations. *Int. J. Climatol.* **2017**, *38*, 269–289. [[CrossRef](#)]
26. Remer, L.A.; Kaufman, Y.J.; Tanre, D.; Tanre, D.; Mattoo, S.; Chu, D.A.; Martins, J.V.; Li, R.R.; Ichoku, C.; Levy, R.C.; et al. The MODIS aerosol algorithm, products and validation. *J. Atmos. Sci.* **2005**, *62*, 947–973. [[CrossRef](#)]
27. Aloysius, M.; Mohan, M.; Parameswaran, K.; George, S.K.; Nair, P.R. Aerosol transport over the Gangetic basin during ISRO-GBP land campaign-II. *Ann. Geophys.* **2008**, *26*, 431–440. [[CrossRef](#)]
28. Kim, S.W.; Yoon, S.C.; Jefferson, A.; John, A.; Ogren, E.G.D.; Won, J.G.; Young, S.G.; Byung, L.; Hand, J.S. Aerosol optical, chemical and physical properties at Gosan, Korea during Asian dust and pollution episodes in 2001. *Atmos. Environ.* **2005**, *39*, 39–50. [[CrossRef](#)]
29. Ricchiazzi, P.; Yang, S.; Gautier, C.; Sowle, D. SBDART: A Research and Teaching software tool for plane-parallel radiative transfer in the Earth’s Atmosphere. *Bull. Am. Meteorol. Soc.* **1998**, *79*, 2101–2114. [[CrossRef](#)]
30. Hess, M.; Koepke, P.; Schulte, I. Optical properties of aerosols and clouds: The software package OPAC. *Bull. Am. Meteorol. Soc.* **1998**, *79*, 831–844. [[CrossRef](#)]
31. Lau, K.M.; Kim, K.M.; Hsu, C.N.; Holben, B.N. Possible influences of air pollution, dust and sandstorms on the Indian monsoon. *WMO Bull.* **2009**, *58*, 22–30.
32. Bevan, S.L.; North, P.R.J.; Grey, W.M.F.; Los, S.O.; Plummer, S.E. Impact of atmospheric aerosol from biomass burning on Amazon dry-season drought. *J. Geophys. Res.* **2009**, *114*. [[CrossRef](#)]
33. Levinson, D.H.; Lawrimore, J.H. *State of the Climate in 2007*; Arguez, A., Diamond, H.J., Fetterer, F., Horvitz, A., Levy, J.M., Eds.; World Meteorological Organization, 2009; pp. 1–193. Available online: https://library.wmo.int/doc_num.php?explnum_id=9763 (accessed on 17 September 2021).

34. Kaskaoutis, D.; Rashki, G.; Houssos, E.E.; Goto, D.; Nastos, P.T. Extremely high aerosol loading over Arabian Sea during June 2008: The specific role of the atmospheric dynamics and Sistan dust storms. *Atmos. Environ.* **2014**, *94*, 374–384. [[CrossRef](#)]
35. Pandya, M.R.; Singh, R.P.; Dadhwal, V.K. A signal of increased vegetation activity of India from 1981 to 2001 was observed using satellite-derived fraction of absorbed photosynthetically active radiation. *Curr. Sci.* **2004**, *87*, 1122–1126.
36. Venkataraman, C.; Habib, G.; Eiguen-Fernandez, A.; Miguel, A.H.; Friedlander, S.K. Residential biofuels in South Asia: Carbonaceous aerosol emissions and climate impacts. *Science* **2005**, *307*, 1454–1456. [[CrossRef](#)]
37. Schuster, G.L.; Dubovik, O.; Holben, B.N. Ångström exponent and bimodal aerosol size distributions. *J. Geophys. Res.* **2006**, *111*. [[CrossRef](#)]
38. Gautam, R.; Hsu, N.C.; Lau, K.M.; Kafatos, M. Aerosol and rainfall variability over the Indian monsoon region: Distributions, trends and coupling. *Ann. Geophys.* **2009**, *27*, 3691–3703. [[CrossRef](#)]
39. Singh, R.P.; Dey, S.; Tripathi, S.N.; Tare, V. Variability of aerosol parameters over Kanpur, northern India. *J. Geophys. Res.* **2004**, *109*. [[CrossRef](#)]
40. Dubovik, O.; King, M.D. A flexible inversion algorithm for retrieval of aerosol optical properties from Sun and Sky Radiance. *J. Geophys. Res.* **2000**, *105*, 20673–20696. [[CrossRef](#)]
41. Dubovik, O.; Holben, B.N.; Eck, T.F.; Smirnov, A.; Kaufman, Y.J.; King, M.D.; Tanré, D.; Slutsker, I. Variability of absorption and optical properties of key aerosol types observed in worldwide locations. *J. Atmos. Sci.* **2002**, *59*, 590–608. [[CrossRef](#)]
42. Dey, S.; Tripathi, S.N.; Singh, R.P.; Holben, B.N. Influence of dust storms on the aerosol optical properties over the Indo-Gangetic basin. *J. Geophys. Res.* **2004**, *109*. [[CrossRef](#)]
43. Prasad, A.K.; Singh, S.; Chauhan, S.S.; Srivastava, M.K.; Singh, R.P.; Singh, R. Aerosol radiative forcing over the Indo-Gangetic plains during major dust storms. *Atmos. Environ.* **2007**, *41*, 6289–6301. [[CrossRef](#)]
44. Kumar, R. *Characterization of Aerosol Optical Properties Using Satellite and Ground-Based Solar Radiation Extinction Studies over Indian Regions*; Career Point University: Kota-Rajasthan, India, 2019; pp. 1–141.